Constraining relativistic models through heavy ion collisions

D.P.Menezes,[1] C. Providência,[2] M. Chiapparini,[3] M.E. Bracco,[3] A. Delfino,[4] and M. Malheiro[4,5]

[1]*Depto de Física - CFM - Universidade Federal de Santa Catarina Florianópolis - SC - CP. 476 - CEP 88.040 - 900 - Brazil*
[2]*Centro de Física Teórica - Dep. de Física - Universidade de Coimbra - P-3004 - 516 - Coimbra - Portugal*
[3]*Instituto de Física - Universidade do Estado do Rio de Janeiro - Rua São Francisco Xavier, 524 - CEP 20550-900 - RJ - Brazil*
[4]*Depto de Física - Universidade Federal Fluminense - Niterói - CEP 24210-150 - RJ - Brazil*
[5]*Depto de Física - Instituto Tecnológico de Aeronáutica, CTA - CEP 12228-900 São José dos Campos - SP - Brazil*

Relativistic models can be successfully applied to the description of compact star properties in nuclear astrophysics as well as to nuclear matter and finite nuclei properties, these studies taking place at low and moderate temperatures. Nevertheless, all results are model dependent and so far it is unclear whether some of them should be discarded. Moreover, in the regime of hot hadronic matter very few calculations exist using these relativistic models, in particular when applied to particle yields in heavy ion collisions. In the present work we comment on the known constraints that can help the selection of adequate models in this regime and investigate the main differences that arise when the particle production during a Au+Au collision at RHIC is calculated with different models.

PACS number(s): 21.65.+f, 24.10.Jv, 95.30.Tg

I. INTRODUCTION

Relativistic models have been widely used in order to describe nuclear matter, finite nuclei and stellar matter properties. Many variations of the well known quantum hadrodynamic model [1] have been developed and used along the last decades. Some of them rely on density dependent couplings between the baryons and the mesons [2, 3, 4, 5, 6] while others use constant couplings [7, 8, 9]. Still another possibility of including density dependence on the lagrangian density is through derivative couplings among mesons and baryons [10, 11, 12] or the coupling of the mediator mesons among themselves [13].

All these quantum hadronic models have under control the fitting of the infinite nuclear matter binding energy at the experimental saturation density (ρ_0). Their results are around $16MeV$ and $0.15fm^{-3}$, respectively. However at the level of nuclear matter, they predict different values for other physical quantites, as for instante, incompressibility (K), effective nucleon mass, scalar and vector potentials, critical temperature (T_c), etc. If applied for finite nuclei, these models also present discrepancies on nuclear spectra. The efforts to find some correlations among observables of infinite nuclear matter and finite nuclear results, lead to interesting conjectures. One is that there is a correlation between the effective nucleon mass (M^*) at the saturation nuclear matter density and the spin-orbit splitting for several nuclei [14], for different quantum hadronic models. This correlation states that good theoretical L-S splittings for several finite nuclei are obtained if M^* lies between 0.58 and 0.62. Other correlation was also proposed to connect T_c with K, M^* and ρ_0 [15].

There is a strong correlation between compact star properties and some of the nuclei properties. Relativistic model couplings are adjusted in order to fit expected nuclei properties such as binding energy, saturation density, compressibility and energy symmetry at saturation density, particle energy levels, etc. Once the same relativistic model is extrapolated to higher densities as in stellar matter or higher temperatures as in heavy-ion collisions or even to lower densities as in the nuclear matter liquid gas phase transitions [16], they can and indeed provide different information. Hence, experimental contraints obtained either from polarized electron scattered from a heavy target, from heavy-ion collisions at different energies or from astronomical observations are very important in order that adequate models are chosen and inadequated ones are ruled out. In what follows we discuss some of the already existing constraints and the relation between equations of state (EoS) used to describe stellar matter and hadronic matter.

The relation between neutron star properties which are obtained from specific EoS and the neutron skin thickness has long been a topic of investigation in the literature. The difference between the neutron and the proton radii, the neutron skin thickness, is linearly correlated with the pressure of neutron matter at sub-nuclear densities. This is so because the properties of neutron stars are obtained from appropriate EoS (very isospin asymmetric due to the β- equilibrium constraint) whose symmetry energy depends on the density and also controls the size of the neutron skin thickness in heavy and asymmetric nuclei, as ^{208} Pb, for instance. In [17] it was shown that the models that yield smaller neutron skins in heavy nuclei tend to yield smaller neutron star radii due to a softer EoS. In [18] it was shown that the neutron skin thickness indeed give hints on the equations of state that are suitable to describe neutron stars. A correlation between the slope of the symmetry energy and the neutron skin thickness, previously found for Skyrme-type models [19], was also observed within relativistic models [18]. Unfortunately a precise measurement of the neutron skin thickness is still under way.

Neutron stars are believed to have a solid crust formed by nonuniform neutron rich matter in β-equilibrium above a liquid mantle. In the inner crust nuclei coexist with a gas of neutrons which have dripped out. The properties of this crust as, for instance, its thickness and pressure at the crust-core interface depend a lot on the density dependence of the EoS used to describe it [20]. On the other hand, it is well known [21, 22] that the existence of phase transitions from liquid to gas phases in asymmetric nuclear matter (ANM) is intrinsically related with the instability regions which are limited by the spinodals. Liquid-gas phase transition in ANM can lead to an isospin distillation phenomenon, characterized by a larger proton fraction in the liquid phase than in the gas phase. In [23] the spinodal sections for two relativistic models, one with constant couplings known as NL3 [7] and another with density dependent couplings we usually refer to as TW, were obtained. The curve that represent the proton versus neutron densities for β-equilibrium matter was represented in the same plot and one can see that it always crosses the spinodal section at $T = 0$. This means that a liquid-gas phase transition occurs at the crust of a cold neutron star giving rise to a nonhomogeneous region. For higher temperatures this effect generally does not occur meaning that the outer layer of a hot compact star is homogeneous. For $T = 10$ MeV, for instance, the two models investigated gave contradictory information as for the NL3 the crossing was observed and for the TW it was not. More information is then required so that the correct picture can be depicted and the wrong EoS ruled out.

Compact star properties can be computed from the solution of the Tolman-Oppenheimer-Volkoff (TOV) equations [24] once they are supposed to be spherically symmetric and static. The input to the TOV equations is the EoS chosen to describe the stellar matter. The determination of neutron star properties obtained from the measureament of the gravitational redshift of spectral lines produced in neutron star photosphere provides a direct constraint on the mass-to-radius ratio. Some time ago a redshift of 0.35 from three different transitions of the spectra of the X-ray binary EXO0748-676 was obtained in [25]. This redshift corresponds to $M/R = 0.15 M_{\odot}/Km$. The 1E 1207.4-5209 neutron star, which is in the center of the supernova remnant PKS 1209-51/52 was also observed and two absorption features in the source spectrum were detected [26]. These features were associated with atomic transitions of once-ionized helium in the neutron star atmosphere with a strong magnetic field. This interpretation leads to a redshift of the order of 0.12-0.23, considerably lower than the one in [25]. This readshift imposes another constraint to the mass to radius ratio given by $M/R = 0.069 M_{\odot}/Km$ to $M/R = 0.115 M_{\odot}/Km$. However, the interpretation of the absorption features as atomic transition lines in [26] is controversial: an alternative interpretation [27, 28] is that the absorption features are cyclotron lines, which imply no obvious constraint on the EoS. In previous works [29, 30, 31] many EoS were tested against these two possible constraints. While all EoS studied so far are consistent with the measurement proposed by [26], many of them are excluded if the redshift found in [25] provides the only possible constraint. As an example we plot the mass and radii obtained from different EoS in Fig. 1, where we have added the line corresponding to the more restrictive constraint (top straight line).

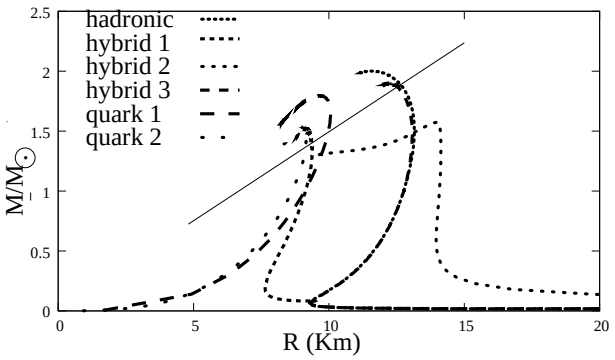

FIG. 1: Mass-radius plots for one hadronic, three hybrid and two quark stars.

The hadronic star [32] was built with the inclusion of 8 baryons within the non-linear Walecka model and parametrization GM1 [9] given in I. The hybrid stars were obtained with the same model and parametrization as above for the hadron phase and different models for the quark phase. Hybrid 1 [33] mixed phase contained the MIT bag model [35] with $Bag = (160\,\mathrm{MeV})^4$, hybrid 2 [33] the color flavored locked phase (CFL) [36] again with $Bag = (160\,\mathrm{MeV})^4$ and hybrid 3 [37] the Namb-Jona-Lasinio (NJL) model [38]. The quark star properties were obtained for the CFL with the same bag parameter as above and called quark 1 and with the NJL model and called quark 2 [33]. One can notice that while hybrid 2 star is excluded, hybrid 1 and hybrid 3 stars remain valid. The hadronic and quark stars remain as possible candidates.

Electron-positron pairs can be emitted from bare quark stars [34] and this dominant emission requires the existence of a surface layer of electrons tied to the star by a strong electric field. While the electron chemical potential of a quark star described by the MIT bag model is very low (less than 20 MeV), the NJL model gives much higher values reaching 100 MeV inside the star [39].

A very recent paper [40] reported a series of possible constraints used separately to analyse relativistic and non-relativistic equations of state applied to neutron stars. The authors mention a relation derived in [41] that correlates gravitational and baryonic neutron star masses and the measurement of Pulsar A moment of inertia [42] which excludes some of the standard mean field relativistic models.

From the above considerations, one can see that different relativistic models in the description of compact stars provide different information. In order to identify the

possible constituents of compact objects and, in this way, rule out some of the relativistic models, more astronomical observations are necessary.

Another attempt in the direction of choosing appropriate models is discussed in the present work in the high temperature regime produced in heavy ion collisions. For this reason we consider Au-Au collisions at RHIC/BNL and analyse the hadron abundances and particle ratios in order to determine the temperature and baryonic chemical potential of the possibly present phase transition. The possibility that a quark-gluon plasma (QGP) could be formed in heavy ion collisions arose when quantum chromodynamics (QCD) at finite temperature and high densities became a topic of increasing interest due to the discovery of asymptotic freedom about 30 years ago. In cosmology, the relevant conditions for QGP formation occur $10\,\mu$s after the Big-Bang theory; nuclear matter first appears after about 1 ms. In laboratory searches for QGP, in large colliders around the world (RHIC/BNL, ALICE/CERN, GSI, etc), experimentalists are trying to do the opposite: to convert hadronic matter at sufficiently high temperatures into QGP.

A first step towards the interpretation of data collected during a Pb+Pb collision at the SPS was taken in [43], where the authors have used a statistical model which assumes chemical equilibration to find the temperature and baryon chemical potential that provide a best fit to the data obtained by the NA49 [44] and WA97 [45] collaborations. They concluded that the chemical freeze-out temperature was $T = 168 \pm 2.4$ MeV and the corresponding baryon chemical potential was $\mu_B = 266 \pm 5$ MeV. Lattice Monte Carlo simulations of QCD at vanishing baryon density gives a very similar estimate, i.e., $T = 170 \pm 8$ MeV [46]. Latter on, the same model was used to analyse the particle production yields measured in central Au+Au collision at RHIC [47] and the authors obtained $T = 174 \pm 7$ MeV and $\mu_B = 46 \pm 5$ MeV. In both cases [43, 47] they used the free Fermi and Boson gas approximations where the interaction among the baryons and mesons were neglected and there were only the above mentioned independent parameters, i.e., the temperature and baryon chemical potential. Three conservation laws were imposed: of the baryon number, the strangeness and the electric charge. While the temperatures found were of the same order, the very different chemical potentials imply different baryon density. In a more recent paper [48], a simple relativistic selfconsistent chiral model, where the nuclear interaction was included, was employed to analyse the Au+Au collision at RHIC once again. The results depend on the parametrizations used but they found a lower temperature around $T = 155$ MeV and the baryon chemical potential of the order of $\mu_B = 51$ MeV. The authors claim that the fitted chemical freeze-out temperatures and chemical potentials depend on the order of the phase transition and suggest that at RHIC the system emerges after the phase transition.

In the present work we revisit the same data and analyse them with the help of more sofisticated relativistic models within a mean field approach. We use four parametrizations of the non-linear Walecka model [1], namely NL3 [7], TM1 [8], GM1 and GM3 [9], one model with implicit density dependence through meson field couplings, the NL$\omega\rho$ [13] and two different parametrizations of a density dependent hadronic model, the TW [3] and the DDME1 [5]. Similar investigations were performed in [49] within one of the parametrizations mentioned below (GM1) and the best fit resulted in $T = 143.9$ MeV and $\mu_B = 25.07$ MeV. We need to understand how model dependent these numbers are. Hence, for comparison, we also investigate the results obtained within a model containing the eight lightest baryons (baryonic octet) without any interaction and then with the baryonic octet plus extra ten baryons (baryonic decuplet) also without interaction to try to understand how important the interaction at low densities are. We implemented a fit based on the minimum value of the quadratic deviation as in [43] in order to obtain the temperature and chemical potential for each model. The paper is organized as follows: in section II we show the lagrangian densities of the models considered and describe the formalism used; in section III we present and discuss the results; in section IV we draw our final conclusions.

II. FORMALISM

In the following we review the basic formulae of the models we use. Just the Lagrangian density and the main expressions for densities and chemical potentials are given. If one wants to follow the analytical calculations in detail, please refer to [1, 18, 50, 51], among many other papers in the literature.

A. Different parametrizations for the non-linear Walecka model

The Lagrangian density that incorporates many parametrizations of the non-linear Walecka model (NLWM) [1, 7, 8, 9] and also the extra non-linear $\sigma - \rho$ and $\omega - \rho$ couplings [13] reads

$$\mathcal{L} = \sum_B \bar{\psi}_B \left[\gamma_\mu \left(i\partial^\mu - g_{vB}V^\mu - g_{\rho B}\boldsymbol{\tau}\cdot\mathbf{b}^\mu \right.\right.$$

$$\left.\left. -e\frac{(1+2\tau_{3B})}{2}A^\mu\right) - (M - g_{sB}\phi)\right]\psi_B$$

$$+\frac{1}{2}(\partial_\mu\phi\partial^\mu\phi - m_s^2\phi^2) - \frac{1}{3!}\kappa\phi^3 - \frac{1}{4!}\lambda\phi^4$$

$$-\frac{1}{4}\Omega_{\mu\nu}\Omega^{\mu\nu} + \frac{1}{2}m_v^2 V_\mu V^\mu + \frac{1}{4!}\xi g_v^4 (V_\mu V^\mu)^2$$

$$-\frac{1}{4}\mathbf{B}_{\mu\nu}\cdot\mathbf{B}^{\mu\nu}+\frac{1}{2}m_\rho^2\mathbf{b}_\mu\cdot\mathbf{b}^\mu-\frac{1}{4}F_{\mu\nu}F^{\mu\nu}$$

$$+g_{\rho B}^2\mathbf{b}_\mu\cdot\mathbf{b}^\mu[\Lambda_s g_{sB}^2\phi^2+\Lambda_v g_{vB}^2 V_\mu V^\mu], \qquad (1)$$

where B represents the lightest 18 baryons, ϕ, V^μ, $\mathbf{b}^\mu$ and A^μ are the scalar-isoscalar, vector-isoscalar and vector-isovector meson fields and the photon field respectively, $\Omega_{\mu\nu}=\partial_\mu V_\nu-\partial_\nu V_\mu$, $\mathbf{B}_{\mu\nu}=\partial_\mu\mathbf{b}_\nu-\partial_\nu\mathbf{b}_\mu-\Gamma_\rho(\mathbf{b}_\mu\times\mathbf{b}_\nu)$, $F_{\mu\nu}=\partial_\mu A_\nu-\partial_\nu A_\mu$ and τ_{3B} is the third component of the baryon isospin. The parameters of the model are: the nucleon mass, of the order of $M=939$ MeV, depending on the parametrization used, the masses of the mesons m_s, m_v, m_ρ, also model dependent, the electromagnetic coupling constant $e=\sqrt{4\pi/137}$ and the coupling constants between baryons and mesons

$$g_{sB}=x_{sB}\ g_s,\quad g_{vB}=x_{vB}\ g_v,\quad g_{\rho B}=x_{\rho B}\ g_\rho,$$

where x_{sB}, x_{vB} and $x_{\rho B}$ are equal to 1 for the nucleons and deltas and acquire different values in different parametrizations for the other baryons. In the present work we have used $x_{sB}=0.7$, $x_{vB}=0.783$ and $x_{\rho B}=0.783$ for couplings between mesons and $\Lambda,\Sigma,\Xi,\Sigma^*,\Xi^*$ and $x_{sB}=x_{vB}=x_{\rho B}=0$ between mesons and the Ω.

Non-linear σ terms are also included in all parametrizations through the constants κ and λ and a non-linear ω term is present in the TM1 [8] parametrization through the constant ξ. A density dependence is introduced through the non-linear $\sigma-\rho$ and $\omega-\rho$ couplings [13], just present in the $NL\omega\rho$ model. We have followed the prescription of [17], where the starting point was the NL3 parametrization and the g_ρ coupling was adjusted for each value of the coupling Λ_i studied in such a way that for $k_F=1.15$ fm^{-1} (not the saturation point) the symmetry energy is 25.68 MeV. In the present work we set $\Lambda_s=0$ as in [13]. Other possibilities for this model with $\sigma-\rho$ and $\omega-\rho$ couplings have already been discussed in the literature. All coupling constants are adjusted in order to reproduce the nuclear matter saturation properties given in Table I.

B. Density dependent hadronic model

The Lagrangian density of the density dependent model we use next reads:

$$\mathcal{L}=\sum_B\bar\psi_B\left[\gamma_\mu\left(i\partial^\mu-\Gamma_{vB}V^\mu-\Gamma_{\rho B}\boldsymbol{\tau}\cdot\mathbf{b}^\mu\right.\right.$$

$$\left.\left.-e\frac{(1+2\tau_{3B})}{2}A^\mu\right)-(M-\Gamma_{sB}\phi)\right]\psi_B$$

$$+\frac{1}{2}(\partial_\mu\phi\partial^\mu\phi-m_s^2\phi^2)-\frac{1}{4}\Omega_{\mu\nu}\Omega^{\mu\nu}$$

$$+\frac{1}{2}m_v^2V_\mu V^\mu-\frac{1}{4}\mathbf{B}_{\mu\nu}\cdot\mathbf{B}^{\mu\nu}+\frac{1}{2}m_\rho^2\mathbf{b}_\mu\cdot\mathbf{b}^\mu-\frac{1}{4}F_{\mu\nu}F^{\mu\nu} \qquad (2)$$

where $\Omega_{\mu\nu}$, $\mathbf{B}_{\mu\nu}$ and $F_{\mu\nu}$ are defined after eq.(1). The parameters of the model are again the masses and the couplings, which are now density dependent, i.e., Γ_s replaces g_s, Γ_v replaces g_v and Γ_ρ replaces g_ρ. Once again the relations

$$\Gamma_{sB}=x_{sB}\ \Gamma_s,\quad \Gamma_{vB}=x_{vB}\ \Gamma_v,\quad \Gamma_{\rho B}=x_{\rho B}\ \Gamma_\rho$$

hold and these density dependent couplings Γ_s, Γ_v and Γ_ρ are adjusted in order to reproduce some of the nuclear matter bulk properties shown in Table I, using the following parametrization:

$$\Gamma_i(\rho)=\Gamma_i(\rho_{sat})h_i(x),\quad x=\rho/\rho_{sat}, \qquad (3)$$

with

$$h_i(x)=a_i\frac{1+b_i(x+d_i)^2}{1+c_i(x+d_i)^2},\quad i=s,v \qquad (4)$$

and

$$h_\rho(x)=\exp[-a_\rho(x-1)], \qquad (5)$$

with the values of the parameters m_i, $\Gamma_i(\rho_{sat})$, a_i, b_i, c_i and d_i, $i=s,v,\rho$ given in [3]. This model does not include self-interaction terms for the meson fields (i.e. $\kappa=0$, $\lambda=0$ and $\xi=0$) as in NL3 or TM1 parametrizations for the NLWM.

Two parametrizations of this density dependent hadronic models are discussed next. The original one, that we refer to as TW and a more recent parametrization known as DDME1 [5], also shown to provide a good description for the properties of many stable nuclei.

C. Calculations

We start by applying the Euler-Lagrange equations to the Lagrangian densities and obtaining the mesonic equations of motion. Then a mean field approximation is enforced and the equations of motion, which have to be solved in a self-consistent way become dependent of the baryonic densities. At this point the electromagnetic field is neglected. For the different parametrizations of the non-linear Walecka model, the densities read:

$$\rho_B=(2J_B+1)\int\frac{\mathrm{d}^3p}{(2\pi)^3}(f_{B+}-f_{B-}),\quad \rho=\sum_B\rho_B, \qquad (6)$$

with $M_B^*=M_B-g_{sB}\ \phi$, $B\pm$ stands respectively for baryons and anti-baryons, $E^*(\mathbf{p})=\sqrt{\mathbf{p}^2+M^{*2}}$ and

$$f_{B\pm}=1/\{1+\exp[(E^*(\mathbf{p})\mp\nu_B)/T]\}\ , \qquad (7)$$

where the effective chemical potential is

$$\nu_B=\mu_B-g_{vB}V_0-g_{\rho B}\ \tau_{3B}\ b_0. \qquad (8)$$

The baryon chemical potentials are computed in terms of their quark constituints, i.e., $\mu_n = \mu_u + 2\mu_d$ and related expressions for the others. As particles and anti-particles have to be computed separately for the calculation of their yields, after the self-consistent calculation they are calculated as

$$\rho_{B+} = (2J_B + 1) \int \frac{\mathrm{d}^3 p}{(2\pi)^3} f_{B+}, \tag{9}$$

$$\rho_{B-} = (2J_B + 1) \int \frac{\mathrm{d}^3 p}{(2\pi)^3} f_{B-}. \tag{10}$$

where $J_B = 1/2$ and $3/2$ respectively for the baryonic octet and decuplet. For the density dependent hadronic model, the expressions are very similar except for the effective mass $M_B^* = M_B - \Gamma_{sB}\, \phi$ and the effective chemical potential

$$\nu_B = \mu_B - \Gamma_{vB} V_0 - \Gamma_{\rho B}\ \tau_{3B}\ b_0 - \Sigma^R_{0\,TW}, \tag{11}$$

where the rearrangement term $\Sigma^R_{0\,TW}$ is given by

$$\Sigma^R_{0\,TW} = \sum_B \left[\frac{\partial \Gamma_{vB}}{\partial \rho} \rho_B V_0 + \frac{\partial \Gamma_{\rho B}}{\partial \rho} \tau_{3b}\ \rho_B\ b_0 \right.$$

$$\left. - \frac{\partial \Gamma_{sB}}{\partial \rho} \rho_{sB} \phi_0, \right]. \tag{12}$$

Moreover, as we are interested in obtaining also the production of pions and kaons, they are introduced through Bose-Einstein distribution functions

$$\rho_i = \frac{2J_M + 1}{2\pi^2} \int_0^\infty p^2 dp \left[\frac{1}{exp[(E_i - \mu_i)/T] - 1} \right], \tag{13}$$

where $i = \pi^+, \pi^-, \pi^0, K^+, K^-, K^0, \bar{K}^0$, and the corresponding vector mesons ρ and K^*, with $J_M = 0$ and 1. $E_i = \sqrt{p^2 + m_i^2}$ and the chemical potencials are again written in terms of their quark constituints, namely, $\mu_{\pi^+} = \mu_u - \mu_d$, $mu_{K^+} = \mu_u - \mu_s$ and so on. We have considered that they behave like a free gas and their properties are not changed due to their interaction with matter and, therefore, the fraction of produced mesons is determined statisitically from their free space properties.

In order to obtain the particle yields and respective densities three conserved quantities are considered: the total strangeness is set to zero, the total number of baryons in a Au+Au collision is $N_B = 2(N + Z) = 394$ and the total isospin is $I_3 = (Z - N)/2 = -39$. Our code deals with 6 unknows, the three meson fields and the three independent quark chemical potentials ($\mu_q, q = u, d, s$), solved in a self-consistent manner.

Finally, as a last test, we have disregarded the interactions by setting all couplings equal to zero. We have also performed the same test, i.e., for free Fermi particles and including the ten baryons with total spin 3/2, as suggested in [48]. We next analyse our results.

III. RESULTS

As already mentioned, in obtaining our results we have fixed the relations between the baryons and the mesons as $x_{sB} = 0.7$, $x_{vB} = 0.783$ and $x_{\rho B} = 0.783$, except for the nucleons and deltas, when they are 1 and for the Ω's, when they are zero. We have verified that other choices give slightly different results but have decided to fix just one possibility to restrict our test to the model differences.

As stated in the Introduction, we have implemented a χ^2 fit as in [43] in order to obtain the temperature and chemical potential for each model. In Table II we show our results for the different models studied corresponding to the temperature and chemical potential that for each model give the minimum value of the quadratic deviation χ^2:

$$\chi^2 = \sum_i \frac{(\mathcal{R}_i^{exp} - \mathcal{R}_i^{theo})^2}{\sigma_i^2}, \tag{14}$$

and

$$q^2 = \sum_i \frac{(\mathcal{R}_i^{exp} - \mathcal{R}_i^{theo})^2}{(\mathcal{R}_i^{theo})^2}, \tag{15}$$

where $\mathcal{R}_i^{exp}$ and $\mathcal{R}_i^{theo}$ are the i^{th} particle ratio given experimentally and calculated with our models and σ_i represents the errors in the experimental data points.

In obtaining the best fit values for the temperature and chemical potentials, we have used the experimental ratios appearing in Table II four times for $\bar{p}/p$, twice for π^-/π^+ and four times for K^-/K^+, all with the same weight. We have also taken into account the K^{0*}/h^- and $\bar{K}^{0*}/h^-$ ratios, where h^- is the net sum of all negative electrically charged hadrons. Instead we could have taken the mean value of the measured values and a statistical average value of the errors. We have checked that the results were similar.

One can observe from Table II that we have found incredibly good agreements between experimental data and all tested models. The only exceptions are the free octet and free octet+decuplet models that cannot describe the $\bar{p}/\pi^-$ ratio. Although the inclusion of the decuplet improves the result, it remains far behind the experimental value. These results show that a proper treatment of the interaction has to be considered. In [43], to account for the repulsive interaction between particles an eigenvolume was assigned to all particles. We have obtained approximately the same freeze-out temperature for all models, namely, $\simeq 146.5 - 152.5$ MeV. The higher limit is close to the value obtained with two parametrizations in [48]. As for the chemical potentials, our results are very model dependent. While all four parametrizatins of the NLWM μ_B predict a similar chemical potential $\sim 47 - 48$ MeV, equal or slighlty lower than the prediction of [48], where the encountered value lies between 48.3 and 54.6

MeV, the density dependent models predict larger values, respectively 59 and 62.5 for DDME1 and TW. To test the importance of including the interaction between particles we have set the couplings to zero. We have obtained a worse χ^2 value compared with the values obtained when interactions are included. Although we get a similar freeze-out temperature, the chemical potentials obtained with no interation are 15-20 MeV smaller.

In Table II we include other ratios not yet measured. We conclude that they are not very sentive to the model except $\bar{\Omega}/\Omega$. The results that are worse reproduced involve mesons, $K-/\pi-$. This seems to indicate that our treatment of the mesons, with constituent masses equal to the vacuum values, is too naive and an improvement should be considered. We have checked that, if we renormalize the mass of the mesons according to the results given in [48] namely, consider the pion and kaon mass 1.1 times the vacuum mass and the K^* mass 0.9 of the vaccuum mass we would get $\chi^2 = 5.3$ and $T = 149.5$ MeV, $\mu_B = 48.75$MeV for the NL3 parametrization.

For the sake of completeness, in Table III we display a sample of hadron effective masses. In this table N stands for nucleons. One can see that, with very few exceptions, they are basically model independent and the influence of the medium is rather low for all baryons, excluding the nucleons. For nucleons the effective mass is at most 15% smaller than the vacuum values. For the other hyperons we get 5-6% reduction. These masses seem to show that the freeze out occurs below the critical temperature. This means that the freeze-out occurs at a temperature below the phase transition to a massless baryon phase.

IV. CONCLUSIONS

In the present work we discussed the necessity of finding constraints able to discard or select appropriate relativistic models. As all models are parametrized to fix nuclear matter saturation properties, once they are extrapolated to lower or higher densities or finite temperature, all sorts of results can turn up. Concerning astronomical measurements, observations that could help in ruling out possible mass-radius relations are most welcome. Constraints can also come from the measurement of a precise neutron skin thickness or from heavy ion collisions, the topic of our calculations here.

By analysing the particle densities and production yields obtained in a Au+Au collision at RHIC we have verified that all models describe the data in a similar way and therefore these data can not be used to establish a constraint. This is due to the fact that the chemical potential and consequently, the baryonic density involved in the hadronization process are very low. We have also confirmed that in order to improve the fit we must go beyond the the naive way mesons were included.

The analysis of the results of the Pb+Pb collision at SPS may be more adequate in the search for constraints to different models since, at least, with thermal models, the chemical potential seems to be much larger. This work is under investigation and, if proved to be an adequate choice, some improvements can be done for the achievement of a better description. The inclusion of strange mesons as mediators of the hyperons [53], responsible for explaining the strongly attractive hyperon-hyperon interaction as observed in double Λ hypernuclei will certainly influence the densities of particles containing strangeness. Also, the inclusion of the scalar isovector virtual $\delta(a_0(980))$ field, that introduces in the isovector channel the structure of relativistic interactions and affects the behavior of the system at high densities or high temperatures [29] can also bring some modifications. Still other relativistic models as the quark-meson-coupling model (QMC) [54] that presents a quarkionic structure inside the hadrons should be investigated. These calculations are already under way. On the other hand, more data is also required.

ACKNOWLEDGMENTS

This work was partially supported by CNPq(Brazil) and FEDER/FCT (Portugal) under the projects POCI/FP/63918/2005 and PDCT/FP/63912/2005.

[1] B. Serot and J.D. Walecka, *Advances in Nuclear Physics* 16, Plenum-Press, (1986) 1.
[2] H. Lenske and C. Fuchs, Phys. Lett. **B 345**, 355 (1995); C. Fuchs, H. Lenske and H.H. Wolter, Phys. Rev. **C 52**, 3043 (1995).
[3] S. Typel and H. H. Wolter, Nucl. Phys. **A656**, 331 (1999).
[4] T. Gaitanos, M. Di Toro, S. Typel, V. Baran, C. Fuchs, V. Greco and H. H. Wolter, Nucl. Phys. **A732**, 24 (2004).
[5] T. Niksic, D. Vretenar, P. Finelli and P. Ring, Phys. Rev. **C 66**, 024306 (2002); D. Vretenar, T. Niksic and P. Ring, Phys. Rev. **C 68**, 024310 (2003).
[6] G.E. Brown and M. Rho, Phys. Rev. Lett. **66**, 2720 (1991).
[7] G. A. Lalazissis, J. König and P. Ring, Phys. Rev. C **55**, 540 (1997).
[8] K. Sumiyoshi, H. Kuwabara, H. Toki, Nucl. Phys. **A 581**, 725 (1995).
[9] N. K. Glendenning, Compact Stars, Springer-Verlag, New-York, 2000.
[10] A. Delfino, C. T. Coelho, M. Malheiro, Phys. Rev. **C 51**, 2188 (1995)
[11] A. Delfino, C. T. Coelho, M. Malheiro, Phys. Lett. **B 345**, 361 (1995)
[12] M. Chiapparini, A. Delfino, M. Malheiro, A. Gattone Z. Phys **A 357**, 47 (1997)

[13] C.J. Horowitz and J.Piekarewicz, Phys. Rev.**C 64**, 062802R (2001); J.K. Bunta and S. Gmuca, Phys. Rev. C **68**, 054318 (2003); J.K. Bunta and S. Gmuca, Phys. Rev. C **70**, 054309 (2004).

[14] R. J. Furnstahl, J. J. Rusnak, B. D. Serot, Nucl. Phys. A **632**, 607, (1998).

[15] J. B. Natowitz et al, Phys. Rev. Lett.**89**, 212701 (2002).

[16] M. Malheiro, A. Delfino, C. T. Coelho, Phys. Rev. **C 58**, 426 (1998).

[17] C.J. Horowitz and J.Piekarewicz, Phys. Rev. Lett. **86**, 5647 (2001).

[18] S.S. Avancini, J.R. Marinelli, D. P. Menezes, M.M. W. Moraes and C. Providência, *Phys. Rev.* **C 75** (2007) 055805.

[19] L. Chen, C.M. Ko and B. Li, nucl-th/0610057.

[20] F. Duchoin and Haensel, Phys. Lett. **B 485**, 107 (2000).

[21] Ph. Chomaz, C. Colonna and J. Randrup, Phys. Rep. **389**, 263 (2004).

[22] S.S. Avancini, L. Brito, D. P. Menezes and C. Providência, Phys. Rev. **C 70**, 015203 (2004).

[23] S.S. Avancini, L. Brito, Ph. Chomaz, D. P. Menezes and C. Providência, Phys. Rev. **C 74**, 024317 (2006).

[24] R.C. Tolman, Phys. Rev. **55** (1939) 364; J.R. Oppenheimer and G.M. Volkoff, Phys. Rev. **55** (1939) 374.

[25] J. Cottam, F. Paerels and M. Mendez, Nature **420**, 51 (2002).

[26] D. Sanwal, G.G. Pavlov, V.E. Zavlin and M.A. Teter, Astrophys. J **574**, L 61 (2002).

[27] G.F. Bignami, P.A. Caraveo,A. De Luca and S. Mereghetti, Nature **423**, 725 (2003).

[28] R.X. Xu,H.G. Wang and G.J. Qiao, Chin. Phys. Lett. **20**, 314 (2003).

[29] D.P. Menezes and C. Providência, Phys. Rev. **C 70**, 058801 (2004)

[30] D.P. Menezes, P.K. Panda and C. Providência, Phys. Rev. **72 C**, 035802 (2005).

[31] D.P. Menezes and D.B. Melrose, Publ. Astron. Soc. Aust. **22**, 292 (2005), astro-ph/0506158.

[32] A. L. Espíndola and D. P. Menezes, Phys. Rev. **C 65**, 045803 (2002); A.M.S. Santos and D.P. Menezes, Phys. Rev. **C 69**, 045803 (2004); R. Cavangnoli and D.P. Menezes, Braz. J. Phys. **35 B**, 869 (2005).

[33] D.P. Menezes, D.B. Melrose, C. Providência and K. Wu, Phys. Rev. **C 73**, 025806 (2006).

[34] D.B. Melrose, R. Fock and D.P. Menezes, Month. Not. Roy. Astr. Soc. **371**, 204 (2006).

[35] A. Chodos, R.L. Jaffe, K. Johnson, C.B. Thorne and V.F. Weisskopf, Phys. Rev. **D 9**, 3471 (1974).

[36] M.G. Alford, K. Rajagopal and F. Wilczek, Nucl. Phys. **B 537**, 443 (1999); M. Buballa and M. Oertel, Nucl. Phys. **A 703**, 770 (2002); M. Alford and S. Reddy, Phys. Rev. D **67**, 074024 (2003).

[37] D.P. Menezes and C. Providência, Phys. Rev. **C 68**, 035804 (2003); D.P. Menezes and C. Providência, Phys. Rev.**C 69**, 045801 (2004).

[38] Y. Nambu and G. Jona-Lasinio, Phys. Rev. **122**, 345 (1961); **124**, 246 (1961).

[39] D.P. Menezes, C. Providência and D.B. Melrose, J. Phys. **G**: Nucl. Part. Phys. **32**, 1981 (2006).

[40] J. Rikovska Stone, P.A.M. Guichon, H.H. Matevosyan and A.W. Thomas, to appear in Nucl. Phys. (2007).

[41] Ph. Podsiadlowski, J.D.M. Dewi, P. Lesaffre, J.C. Miller, W.G. Newton and J. Rikovska Stone, Mon. Not. R. Astron. Soc. **361**, 1243 (2005).

[42] J.M. Lattimer and b.F. Schultz, ApJ **629**, 979 (2005).

[43] P. Braun-Munzinger, I. Heppe and J. Stachel, Phys. Lett. **B 465**, 15 (1999).

[44] NA49 Collaboration, H. Appelshäuser et al., Phys. Lett. **B 444**, 523 (1998); F. Gabler, J. Phys. **G 25**, 199 (1999) and many others.

[45] WA Collaboration, E. Andersen et al., J. Phys. **G 25**, 171 (1999); E. Andersen et al., Phys. Lett. **B 449**, 401 (1999) and many others.

[46] F. Karsch, Nucl. Phys. **B** - Proceedings Supl. **83-4**, 14 (2000).

[47] P. Braun-Munzinger, D. Magestro, K. Redlich and J. Stachel, Phys. Lett. **B 518**, 41 (2001).

[48] D. Zschiesche, S. Schramm, J. Schaffner-Bielich, H. Stöcker and W. Greiner, Phys. Lett. **B 547**, 7 (2002).

[49] M. Chiapparini and M.E. Bracco, Int. J. Mod. Phys. **E**, (2007) accepted.

[50] S.S. Avancini and D.P. Menezes, Phys. Rev. **C 74**, 015201 (2006).

[51] D.P. Menezes and C. Providência, astro-ph/0703649.

[52] B. Liu, V. Greco, V. Baran, M. Colonna and M. Di Toro, Phys. Rev. C **65**, 045201 (2002); D.P. Menezes and C. Providência, Phys. Rev. **C 70**, 058801 (2004).

[53] J. Schaffner-Bielich, Phys. Rev. Lett. **89**, 171101 (2002); R. Cavagnoli and D. P. Menezes, Braz. J. Phys. **35 B**, 869 (2005).

[54] P. A. M. Guichon, Phys. Lett. **B 200**, 235 (1988); K. Saito and A.W. Thomas, Phys. Lett. **B 327**, 9 (1994); K. Tsushima, K. Saito, A.W. Thomas and S.V. Wright, Phys. Lett. **B 429**, 239 (1998).

TABLE I: Nuclear matter properties.

ratio	NL3	TM1	GM1	GM3	NL$\omega\rho$			TW	DDME1
	[7]	[8]	[9]	[9]	[13]			[3]	[5]
					$\Lambda_v = 0.01$	$\Lambda_v = 0.02$	$\Lambda_v = 0.025$		
B/A (MeV)	16.3	16.3	16.3	16.3	16.3	16.3	16.3	16.3	16.2
ρ_0 (fm^{-3})	0.148	0.145	0.153	0.153	0.148	0.148	0.148	0.153	0.152
K (MeV)	271	281	300	240	271	271	271	240	244.5
$\mathcal{E}_{sym.}$ (MeV)	37.4	36.9	32.5	32.5	34.9	33.1	32.3	32.0	33.1
M^*/M	0.60	0.63	0.70	0.78	0.60	0.60	0.60	0.56	0.578

TABLE II: Comparison of experimental particle ratios and relativistic mean field models.

ratio	exp. data	exp	NL3 [7]	TM1 [8]	GM1 [9]	GM3 [9]	TW [3]	DDME1 [5]	octet	octet + decuplet
$\bar{p}/p$	0.65±0.07	STAR	0.650	0.646	0.626	0.597	0.656	0.663	0.661	0.649
	0.64±0.07	PHENIX								
	0.60±0.07	PHOBOS								
	0.64±0.07	BRAHMS								
$\bar{p}/\pi^-$	0.08±0.01	STAR	0.075	0.072	0.072	0.063	0.076	0.074	0.039	0.041
π^-/π^+	1.00±0.02	PHOBOS	0.998	0.991	0.999	1.00	1.01	1.01	1.00	1.01
	0.95±0.06	BRAHMS								
K^-/K^+	0.88±0.05	STAR	0.912	0.911	0.907	0.905	0.896	0.900	0.961	0.941
	0.78±0.13	PHENIX								
	0.91±0.09	PHOBOS								
	0.89±0.07	BRAHMS								
K^-/π^-	0.149±0.02	STAR	0.234	0.234	0.242	0.243	0.228	0.227	0.232	0.235
$\bar{\Lambda}/\Lambda$	0.77±0.07	STAR	0.681	0.680	0.666	0.644	0.663	0.675	0.687	0.689
$\bar{\Xi}^-/\Xi^-$	0.82±0.08	STAR	0.746	0.747	0.735	0.711	0.739	0.748	0.714	0.732
K^{0*}/h^-	0.06 ± 0.017	STAR	0.058	0.059	0.063	0.064	0.064	0.063	0.060	0.061
$\bar{K}^{0*}/h^-$	0.058 ± 0.017	STAR	0.053	0.054	0.057	0.058	0.056	0.056	0.057	0.057
$\bar{\Omega}/\Omega$			0.693	0.699	0.715	0.723	0.585	0.586	-	0.784
$\bar{\Omega}/\pi^-$			0.001	0.001	0.002	0.002	0.001	0.001	-	0.001
Λ/h^-			0.021	0.020	0.021	0.020	0.023	0.022	0.013	0.014
Ω/Ξ^-			0.172	0.178	0.195	0.211	0.173	0.174	-	0.250
λ/K^{0*}			0.351	0.341	0.331	0.301	0.363	0.353	0.226	0.228
$\bar{\Xi}^-/\Lambda$			0.226	0.226	0.227	0.221	0.296	0.295	0.241	0.222
$\bar{\Xi}^-/\bar{\Lambda}$			0.332	0.332	0.341	0.343	0.330	0.327	0.312	0.322
$\Xi^-/\bar{K}^-$			0.047	0.045	0.050	0.049	0.048	0.045	0.027	0.030
$\bar{\Xi}^-/\bar{K}^-$			0.035	0.034	0.035	0.033	-	-	0.019	0.022
T(MeV)			149	149	152.	152.8	146.6	146.2	146.4	148.8
μ_b (MeV)			47.5	46.5	47.5	48.	62.8	57.	30.5	32.5
$\rho \times 10^{-3}$ (fm^{-3})			8.37	8.03	9.62	9.95	4.90	4.45	2.41	4.77
χ^2			23.94	24.43	27.99	33.19	22.18	21.83	45.44	41.63
radius (fm)			22.4	22.7	21.38	21.14	26.77	27.65	33.91	27.02

TABLE III: Effective masses obtained with the temperature and chemical potentials given in Table II.

	NL3 [7]	TM1 [8]	GM1 [9]	GM3 [9]	TW [3]	DDME1 [5]
M^*_N/M_N	0.88	0.89	0.90	0.93	0.87	0.87
M^*_Λ/M_Λ	0.93	0.93	0.94	0.96	0.92	0.92
M^*_Σ/M_Σ	0.94	0.94	0.95	0.96	0.93	0.93
M^*_Ξ/M_Ξ	0.94	0.95	0.95	0.96	0.93	0.94
M^*_Δ/M_Δ	0.91	0.92	0.93	0.95	0.90	0.90
$M^*_{\Sigma^*}/M_{\Sigma^*}$	0.94	0.95	0.95	0.95	0.94	0.94
$M^*_{\Xi^*}/M_{\Xi^*}$	0.95	0.95	0.96	0.97	0.94	0.94
M^*_Ω/M_Ω	1.00	1.00	1.00	1.00	1.00	1.00